

LASER GYROSCOPES

PACS numbers: 06.30.Gv; 07.07.Df; 32.60.+i; 42.60.Da
DOI: 10.1070/QE2015v045n02ABEH015539

Zeeman laser gyroscopes

V.V. Azarova, Yu.D. Golyaev, I.I. Savelyev

Abstract. **The history of invention and development of Zeeman laser gyroscopes, specific features of their optical scheme and operation principle are described. The construction and element base of modern laser angular velocity sensors with Zeeman-based frequency biasing are considered. The problems and prospects of their development are discussed.**

Keywords: *Zeeman effect, ring laser, laser gyroscope.*

1. Introduction

The history of optical gyroscopes began as early as in 1913, when the properties of a rotating ring interferometer were studied by Sagnac for the first time. In 1963 after the invention of first lasers the idea of using a ring laser as an optical interferometer appeared. In the process of implementing this idea a number of fundamental advantages of laser gyroscopes (LGs) over mechanical gyroscopes developed at that time were revealed, including the unlimited dynamic range of measured angular velocities, small readiness time, high stability against g-loads, and significant potentialities of improvement and accuracy enhancement.

The presently developed and used LGs may be divided into three main types with different methods of the so-called frequency biasing (creating an artificial frequency separation between the counterpropagating laser waves in the absence of rotation). These methods include mechanical vibration, Zeeman and Faraday effects. The vibrational frequency biasing (dithering) is based on real mechanical rotation (angular vibration) of the gyroscope. It is characterised by high long-term stability, allows the use of high-Q cavities with linear polarisation of generated radiation, and provides the maximal gyroscope precision. However, this type of frequency biasing suffers from a serious drawback, the presence of moving mechanical parts that drastically reduce the gyroscope resistance to external mechanical and environmental disturbances.

The Zeeman and Faraday (magnetooptical) methods of frequency biasing are based on the artificial electrically controlled separation of frequencies of the counterpropagating waves in the gyroscope. The rotation is simulated by introducing a nonreciprocal element into the cavity. In the Zeeman method the role of a nonreciprocal element is played by the active medium itself, the mixture of neon and helium gases. The nonreciprocity in a ring laser is provided by creating circular polarisation of radiation at the expense of making the cavity contour to be nonplanar and applying magnetic field to the active medium. In the Faraday method the nonreciprocity is created by introducing a Faraday cell into the cavity. The parameters of the frequency biasing are determined by electric signals supplied to the nonreciprocal elements, which offers greater flexibility in controlling the frequency bias and achieving the optimal values of the parameters. The most important advantage of gyroscopes with such type of bias is the absence of any moving mechanical parts and high resistance to mechanical and climatic disturbances and the drawback is lower long-term stability of their precision parameters. However, the progress in technology of fabricating dielectric mirrors and antireflection coatings makes it possible to reduce the gap in precision parameters between the gyroscopes with mechanical and magnetooptical frequency biasing.

The present paper is devoted to Zeeman laser gyroscopes (ZLGs) differing from other types of laser gyroscopes in a numbers of valuable qualities. Among them is the monolithic construction, provided by the absence of moving massive parts, the flexible electronically controlled magnetooptical frequency biasing, the high stability of the nonplanar cavity with respect to misalignment of mirrors and the possibility of using the four-wave regime of laser oscillation.

The ZLG history began in 1967 at the Polyus Research Institute (USSR), when the invention certificate for ZLGs was received [1]. In 1969 the first specimen of such a gyroscope was fabricated [2]. By the end of the 1990s a series of ZLGs was developed [3–7], the prototypes of the devices presently in serial production.

At present the development of ZLGs and ZLG-based systems is the laser engineering mainstream at the Polyus Research Institute, and the Institute itself is one of the leaders of domestic laser gyro engineering.

2. Specific features of ZLG operation principle and optical scheme

Similar to other laser gyroscopes, the operation of ZLGs is based on the Sagnac effect, repeatedly and thoroughly considered in the literature [8–18]. Let us consider in more detail the specific features of the ZLG optical scheme and construction.

2.1. Nonplanar optical cavity

ZLGs make use of the four-mirror nonplanar ring cavity schematically shown in Fig. 1.

V.V. Azarova, Yu.D. Golyaev, I.I. Savelyev OJSC 'M.F. Stel'makh Polyus Research Institute', ul. Vvedenskogo 3, 117342 Moscow, Russia; e-mail: azarovav@hotbox.ru, goljaev@bk.ru, i.saveliev@gmail.com

Received 19 April 2014
Kvantovaya Elektronika **45** (2) 171–179 (2015)
Translated by V.L. Derbov

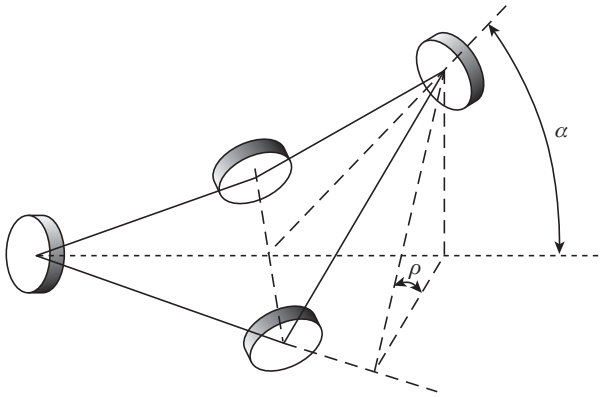

Figure 1. Schematic diagram of a nonplanar cavity with the bending angle α (ρ is the angle between the planes of incidence on the successive mirrors, equal to the angle of beam pattern rotation in a single reflection).

The polarisation, spectral and spatial characteristics of the modes of such a cavity and the radiation of lasers on its basis are considered in Refs [4–7, 19–27]. Its specific feature is the rotation of the laser beam cross-section pattern through the angle ρ, equal to the turn angle of the incidence planes of successive mirrors at each reflection, so that during a roundtrip the laser beam cross-section pattern and, therefore, its electromagnetic field, rotates through the angle equal to the sum of turn angles of successive mirrors. Due to this fact a nonplanar four-mirror cavity with a contour bend angle $\alpha \neq 0$ intrinsically possesses the circular polarisation anisotropy. Since for oblique incidence the mirrors have linear polarisation anisotropy, the polarisation of modes becomes close to circular only at sufficiently large bending angles. The polarisation ellipticity depends on the parameters of polarisation anisotropy of mirrors and the angles, determining the turn of incidence planes of the successive mirrors.

In nonplanar cavities the frequency degeneracy of eigenmodes with orthogonal circular polarisations is removed.

The calculation of polarisation states and frequency spectrum of a nonplanar cavity is based on the matrix equations [4, 27]

$$\widehat{M}\cdot\boldsymbol{E} = \gamma\boldsymbol{E}, \tag{1}$$

where

$$\widehat{M} = \begin{bmatrix} M_{11} & M_{12} \\ M_{21} & M_{22} \end{bmatrix}$$

is the matrix describing the influence of all cavity elements on the light wave circulating in it;

$$\boldsymbol{E} = \begin{pmatrix} E_x \\ E_y \end{pmatrix}$$

is the complex electric vector of the light wave; γ is the eigenvalue of the matrix $\widehat{M}$; and E_x and E_y are the projections of the vector $\boldsymbol{E}$ on the axes of the right-hand rectangular coordinate system with the z axis directed along the direction of wave propagation.

The quantity γ characterises the change in the amplitude and the phase shift of the light wave during the cavity roundtrip. For the cavity eigenmodes the phase shift per roundtrip must be multiple of 2π. The matrix equation (1) is a system of two equations for the projections E_x and E_y. This system of equations has two solutions that correspond to two modes with the orthogonal polarisation of the electric field:

$$\gamma_{1,2} = \frac{1}{2}[\mathrm{Sp}M \pm \sqrt{(\mathrm{Sp}M)^2 - 4\det M}\,], \tag{2}$$

$$\left|\frac{E_x}{E_y}\right|_{1,2} = \frac{M_{12}}{\gamma_{1,2} - M_{11}}. \tag{3}$$

For nonplanar cavities the radicand is always negative, $(\mathrm{Sp}M)^2 - 4\det M < 0$, which leads to the difference of phase shifts per cavity roundtrip and, therefore, of the frequencies of the modes with different polarisation states (the signs '+' and '–' correspond to these states). For one of the counterpropagating waves in a nonplanar cavity with ideal mirrors the roundtrip matrix is equivalent to the matrix of rotation of x and y axes through the angle ρ_Σ:

$$\widehat{M} = \begin{bmatrix} \cos\rho_\Sigma & -\sin\rho_\Sigma \\ \sin\rho_\Sigma & \cos\rho_\Sigma \end{bmatrix} = \widehat{M}(\rho_\Sigma), \tag{4}$$

where ρ_Σ is the total angle of the beam pattern rotation during the roundtrip. Substituting Eqn (4) into Eqns (2) and (3), we obtain $\gamma_{1,2} = \exp(\pm i\rho_\Sigma)$ and $|E_x/E_y|_{1,2} = \exp(\pm i\pi/2) = \pm i$.

Hence, in this approximation the eigenmodes of the nonplanar cavity have the right-hand (RCP) and left-hand (LCP) circular polarisation independent of the pattern rotation angle ρ_Σ, and the phase shift between them is equal to the doubled angle of rotation of axes per roundtrip, $2\rho_\Sigma$. In turn, the frequency difference between the modes with orthogonal polarisation $\nu_c^\pm$ is

$$\nu_c^+ - \nu_c^- = \frac{c}{L}\frac{\rho_\Sigma}{\pi}, \tag{5}$$

where c is the velocity of light and L is the cavity perimeter length. The cavity frequency spectrum and, correspondingly, the frequency shift of the modes with RCP and LCP depend on the bending angle of the cavity optical contour α (Fig. 1) and, therefore, on ρ_Σ. Changing the cavity bending angle, one can obtain the required frequency spectrum. The formation of the frequency spectrum in the cavity for one of the directions of wave propagation is shown in Fig. 2.

In the case of a two-frequency ZLG the major problem is how to provide the maximal possible frequency separation for the orthogonally polarised modes in order to operate with one of them solely. The equidistant spectrum of longitudinal modes corresponds to this requirement. In turn, such a spectrum is provided by the special construction of the cavity, in which the angle of the beam pattern rotation per roundtrip is $\rho_\Sigma = 90°$. For double-frequency gyroscopes such an angle is provided by setting the bending angle as $\alpha = 32°$, the angle between the incidence planes of the two successive mirrors being $\rho = 22.5°$ (see Fig. 1).

In designing four-frequency laser gyroscopes, there arises a problem of optimisation of the frequency separation between the modes with RCP and LCP in order to obtain the four-frequency regime. The ring cavity spectrum of eigenfrequencies shown in Fig. 2 allows the solution of this problem with the bending angle $\alpha = 57°$ and the total rotation angle $\rho_\Sigma = 189°$.

In contrast to planar cavities, the nonplanar one possesses high stability with respect to misalignment, even having plane mirrors. In this case the misalignment tolerance, as well as the

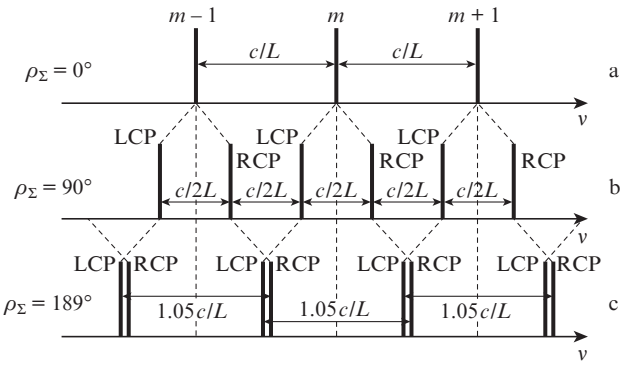

Figure 2. Eigenfrequency spectrum of longitudinal modes of a planar cavity with linear polarisation (a) and four-mirror nonplanar ring cavities having the same perimeter L, belonging to the two-frequency ZLG (b), and the four-frequency ZLG (c) with different total rotation angles ρ_Σ.

frequency spectrum of longitudinal modes, is determined by the angle ρ_Σ. The value of angular misalignments is inversely proportional to $\sin(\rho/2)$, therefore already for $\rho_\Sigma = 90°$, provided that the cavity is of high quality, the deviations of the optical contour from an ideal one are so small that the cavity needs no alignment. The minimal sensitivity to misalignment is observed at $\rho_\Sigma = 180°$.

2.2. Zeeman frequency-biased ring laser

In a ZLG the role of a sensitive element is played by the ring He–Ne laser with a nonplanar cavity, the active medium of which is subjected to the longitudinal magnetic field. The active medium is pumped by a direct-current glow discharge. The highly selective cavity with a high Q-factor provides the laser oscillation in the regime of a single longitudinal mode at the transition $3s_2 - 2p_4$ of neon with the wavelength 633 nm.

Due to the circular anisotropy of the nonplanar ring cavity the laser generates the waves with circular polarisations, and the modes with LCP and RCP appear to be frequency-separated (Fig. 2).

In a single-mode laser only two counterpropagating waves (cw and ccw) of the similar polarisation are generated. In the passive cavity in the absence of rotation they have equal frequencies ($\nu_{cw} = \nu_{ccw}$) and, as a rule, are tuned to the central frequency ν_0 of the gain profile. In the longitudinal magnetic field the gain curve is Zeeman-split, and one gets two gain components, the low-frequency one with the central frequency ν_0^- and the high-frequency one with the central frequency ν_0^+ (Fig. 3). The frequency separation (the frequency difference between the shifted gain profiles) is determined by the expression [19]

$$\delta\nu_0 = \nu_0^+ - \nu_0^- = \frac{eg}{2\pi mc} H, \tag{6}$$

where e is the electron charge; m is the electron mass; H is the magnetic field strength; and g is the Landè factor. Using the tabulated values of the physical constants and the Landè factor for the lasing transition, we obtain $\delta\nu_0 = 3.64\times10^6 H$ (Hz), where H is expressed in oersteds.

Each contour determines the gain only for one of the possible light polarisations, the low-frequency one for LCP wave propagating along the magnetic field, and the high-frequency one for the RCP wave. Due to the mode frequency pulling effect, the frequencies of real waves are shifted towards the centre of the gain profile [28]. Figure 3 shows the frequency shift of the counterpropagating waves with RCP.

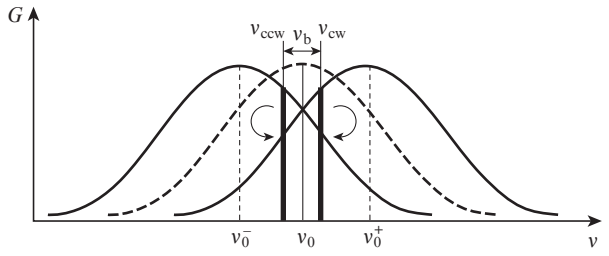

Figure 3. Zeeman splitting of counterpropagating waves (ν_0 is the mode frequency in the absence of the magnetic field, ν_{cw}, ν_{ccw} are the frequencies of the counterpropagating waves split in the magnetic field, and ν_b is the frequency difference between the counterpropagating waves).

The resulting frequency difference between the counterpropagating waves ν_b, referred to as the bias frequency, can be expressed as follows [7]:

$$\nu_b = \nu_{cw} - \nu_{ccw} = 0.94\frac{\Delta\nu_c}{\Delta\nu_D}\frac{G}{\sigma}(\nu_0^+ - \nu_0^-), \tag{7}$$

where $\Delta\nu_D$ and $\Delta\nu_c$ are the laser gain linewidth and the cavity transmission bandwidth, respectively; and G and σ are the gain and loss coefficients of the cavity. The sign of the frequency difference depends on the polarisation of the generated mode.

Using Eqn (6) we transform formula (7) in the following way:

$$\nu_b = \pm 2.63\times10^6\frac{\Delta\nu_c}{\Delta\nu_D}\frac{G}{\sigma}H. \tag{8}$$

For typical ZLG parameters ($\Delta\nu_c$ = 1.5 MHz, $\Delta\nu_D$ = 1.5 GHz. $G/\sigma = 2$, $H = 20$ Oe) we obtain the following values of Zeeman splitting and bias frequency: $2\delta\nu_0 = 7.2\times10^7$ Hz, ν_b = 135 kHz. The method of frequency biasing in a four-frequency ring laser is similar. For this case the scheme of frequency positions and bias frequency formation is shown in Fig. 4.

A more detailed description of the ZLG amplitude–frequency characteristics under the real operating conditions (with the self-saturation, great excess of gain over the losses, etc., taken into account) is given in Refs [21–26].

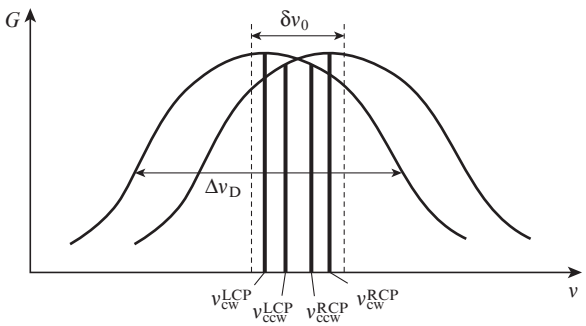

Figure 4. Schematic illustration of the frequency positions and the frequency biasing in a four-frequency Zeeman ring laser.

2.3. Coupling and frequency capture of counterpropagating waves in a ring laser with nonplanar cavity

The physical phenomena leading to the coupling of counterpropagating waves and the capture of their frequency in ring laser gyroscopes were studied in many papers [12, 18, 29–33]. The cause of linear coupling of counterpropagating waves in ring lasers is the backscattering of light by the cavity elements, due to which a small part of the counterpropagating wave is added to each bare (non-scattered) cavity mode. As a result of nonlinear interaction of modes in the active medium the frequencies of the generated waves become closer to each other, and at some (threshold) velocity of rotation the frequency locking of the counterpropagating waves occurs, i.e., the frequencies of the counterpropagating waves become equal. This phenomenon is referred to as the frequency capture of the counterpropagating waves, and the frequency difference, corresponding to the threshold velocity of rotation – as the capture frequency or the capture threshold.

A ring laser with a nonplanar cavity has some specific features related to the circular polarisation of counterpropagating waves. Theoretically, in the absence of depolarisation the backscattered wave must have the circular polarisation, orthogonal to that of the similarly directed fundamental wave, and is unable to interact with it, so that no capture is possible. This effect is called the polarisation decoupling. Practically a significant part of the scattered wave is depolarised, and the capture is always observed. To overcome it in a ZLG the Zeeman frequency biasing is used. Its advantage over the dithering is the complete absence of moving parts, and over other magnetooptical methods – the absence of additional optical elements in the cavity that increase the losses and light scattering. In addition, this method is low-inertial and allows tailoring practically any shape of the frequency bias, including the sign-changing one. An important additional advantage of such frequency bias is the absence of severe requirements to the stability of its amplitude and the possibility of subtracting the bias from the output LG signal at each period of its variation.

In the absence of competition between the counterpropagating waves, when the stable double-direction oscillation exists in the LG, the variation of the counterpropagating waves phase difference Ψ can be described by the approximate equation [32]

$$d\Psi/dt = K\Omega - K\Omega_0 \sin(\Psi + \beta), \tag{9}$$

where K is the scale factor; Ω is the total frequency nonreciprocity of the cavity, including the angular velocity of LG rotation; Ω_0 is the capture frequency; and $\beta = \beta_1 - \beta_2$ is the phase difference of the backscattering coefficients of the counterpropagating waves. The capture frequency is determined by the equation

$$\Omega_0 = (\sigma_1^2 + \sigma_2^2 - 2\sigma_1\sigma_2\cos\beta)^{1/2}, \tag{10}$$

where σ_1, σ_2 are the amplitudes of the backscattering coefficients of the counterpropagating waves, and

$$\sigma_{1,2} = \varepsilon_{1,2} r_{1,2} \frac{cE_{2,1}}{LE_{1,2}}. \tag{11}$$

Here, $\varepsilon_{1,2}$ are the depolarisation coefficients of the backscattered waves; $r_{1,2}$ are the relative coefficients of the total backscattering of the waves into the solid angle of the cavity mode; and $E_{1,2}$ are the field amplitudes of the counterpropagating waves. The depolarisation coefficients are determined, first of all, by the 'smoothness' of the mirror surfaces and the angle of incidence. For the cavities used in ZLGs their value amounts to 0.4–0.6. The coefficients $r_{1,2}$ that enter Eqn (11) are determined by the interference of all waves scattered in the cavity. Depending on their relative phases, the values of $r_{1,2}$ can vary within wide limits, theoretically, from zero to their sum. The phase difference β is determined by the character of the mirror surface scattering centres (if these centres are inhomogeneities of the dielectric constant, then $\beta = 0$, and if the scattering is caused only by the absorption inhomogeneities, then $\beta = \pi$).

In real lasers the mirrors give rise both to absorption and to scattering from the dielectric constant inhomogeneities, so that $\beta \neq 0$ and the capture frequency Ω_0 is practically always nonzero. Assuming the amplitudes and the total backscattering coefficients to be equal for the counterpropagating waves, which is close to the real situation ($\sigma_{1,2} = \sigma$, $r_{1,2} = r$, $\varepsilon_{1,2} = \varepsilon$), and $\beta = \pi/2$, we arrive at the approximate formula for evaluating the capture frequency

$$\Omega_0 \cong \sigma\sqrt{2} = \frac{\varepsilon r c\sqrt{2}}{L}. \tag{12}$$

For the integral scattering into the mode solid angle from all four mirrors $r = (0.66–2)\times10^{-6}$, the depolarisation coefficient $\varepsilon = 0.5$ and the laser perimeter $L = 16$ cm, the capture frequency is equal to $\Omega_0 = (0.3–0.8)\times10^3$ Hz, which is by more than two orders of magnitude greater than the frequency splitting caused by the rotation of the Earth (4.6 Hz). Just for this reason the problem of reducing backscattering and capture effects remains to be the central one throughout the history of laser gyroscope engineering.

The mirror quality improvement can reduce the backscattering and, thus, decrease the capture frequency.

An alternative possibility of reducing the capture frequency is to minimise the total scattered intensity by choosing appropriate relative phases of the waves scattered from the mirrors, which can be implemented by high-precision adjustment of the distances between the mirrors.

Equation (9) has two different solutions depending on the nonreciprocity value Ω. When $\Omega \leqslant \Omega_0$, i.e., in the capture zone, we obviously have $d\Psi/dt = \Delta\nu = 0$. For $\Omega > \Omega_0$, i.e., beyond the capture zone, the solution of Eqn (9) is

$$\Delta\nu = K(\Omega^2 - \Omega_0^2)^{1/2}. \tag{13}$$

The solution (13) is graphically illustrated in Fig. 5.

2.4. Sign-changing Zeeman frequency biasing

The sign-changing modulation of the magnetic field in the active medium leads to the periodic interchange of low- and high-frequency gain profiles (Fig. 3) and, therefore, the periodic sign change of the frequency bias ν_b [see Eqns (7), (8)]. The modulation frequency f_b is usually within the range 200–1000 Hz. By the appropriate processing of the output signal modulated with the frequency f_b it is possible to eliminate (subtract) its sign-changing part, leaving only the signal caused by the useful nonreciprocal effect (i.e., the rotation). This subtraction is executed during one period of modulation that amounts to 1–5 ms, and the frequency bias stability should

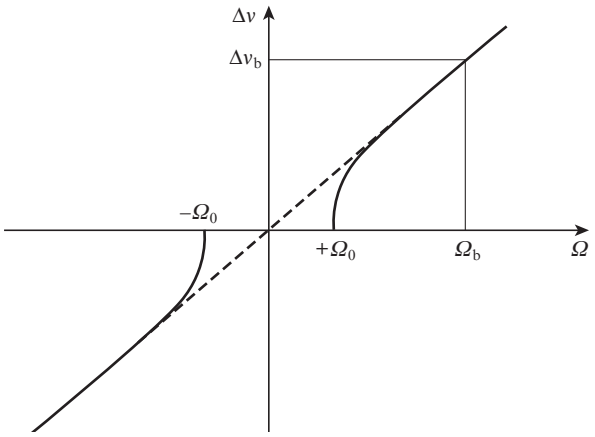

Figure 5. Ideal (dashed line) and real (solid lines) frequency characteristics of a LG; Ω_b is the rotation frequency, corresponding to the bias frequency ν_b.

be provided just during this period of time. This is technically much simpler than in LGs with a constant magnetic field, where this stability must be supported during the entire time of LG operation.

The sign-changing modulation of the frequency bias using the periodic magnetic field gives rise to new physical effects, first of all, to parametric resonances. In real LGs these resonances manifest themselves as the so-called locking zones. The frequency characteristic of a real LG with the sign-changing frequency bias switching rate f_b for $\Omega \ll \Omega_b$ is shown in Fig. 6.

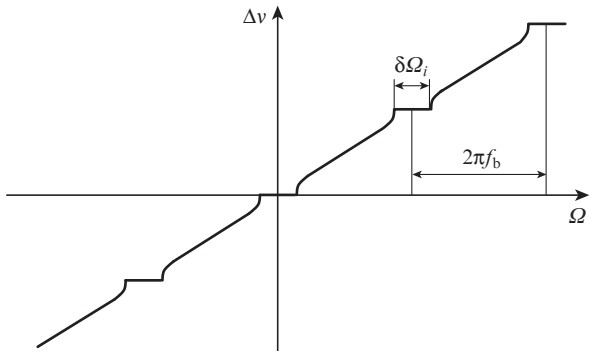

Figure 6. Frequency characteristic of a real LG with sign-changing frequency bias with the switching rate $2\pi f_b$ at $\Omega \ll \Omega_b$. The horizontal 'shelves' correspond to the dynamic locking zones with the width $\delta\Omega_i$ (i is the zone number).

The dynamic locking zones in the LG frequency characteristic are separated by the frequency interval f_b; the number of such zones in the interval $[0; \nu_b]$, i.e., from zero to the bias frequency ν_b, can amount to a few hundreds. The static locking zone coincides with the zeroth dynamic zone.

In the case of sign-changing frequency biasing the equation for the phase difference between the counterpropagating waves takes the form [18]:

$$d\Psi/dt = K\Omega - K\Omega_0 \sin(\Psi + \beta) + \nu_b F(t), \tag{14}$$

where $F(t)$ is the periodic sign-changing function describing the time behaviour of the sign-changing frequency bias.

The widths of the dynamic locking zones $\delta\Omega_i$ in the first approximation are related to the frequency of the static capture zone Ω_0 as

$$\Omega_0^2 = \sum_i (\delta\Omega_i)^2. \tag{15}$$

The quantities $\delta\Omega_i$ are determined by the temporal shape of the sign-changing frequency bias, as well as by the values of ν_b and Ω_0. When the magnetic field is removed ($H = 0$) the dynamic locking zones disappear, and the static capture zone becomes completely restored.

The effect of the dynamic locking zones can be eliminated by introducing the noise into the frequency bias [33].

The second essential component of errors in the laser gyroscope measurement of angular parameters, which is also determined mainly by the coupling of counterpropagating waves via backscattering, is the scale factor nonlinearity. This nonlinearity manifests itself most strongly at the angular velocities close to that corresponding to the bias frequency. The nonlinearity of the dynamic characteristic depends on the shape of the frequency bias. For rectangular shape (meander) in a wide range of angular velocities smaller than the bias frequency ν_b the nonlinearity is quadratic, and the dependence of the scale factor K on Ω can be described by the formula

$$K = K_0[1 - \Delta K(\Omega)], \tag{16}$$

where K_0 is the part of the scale factor, independent of the angular velocity; $\Delta K(\Omega)$ is the scale factor variation determined by the nonlinear dependence on the angular velocity.

In the above approximations

$$K_0 = \frac{4S(1-a)}{\lambda L}, \tag{17}$$

$$\Delta K(\Omega) = \frac{\Omega_0^2 K_0}{2(\Omega_b^2 - \Omega^2)}. \tag{18}$$

Here, S is the area bounded by the projection of the closed optical contour onto the plane, perpendicular to the axis of LG sensitivity to rotation; and a is the coefficient, proportional to the active medium gain. Equation (18) does not allow determination of the scale factor variations at angular velocities near the bias frequency or greater than it.

For more precise description of the dependence of K on the angular velocity in the entire measurement range, including the case $\Omega = \Omega_b$, the theory [19, 20] that describes the frequency and amplitude dependences for the counterpropagating waves in a ring laser with the sign-changing frequency bias is developed and the computer numerical calculations of the ring laser frequency characteristic in the entire dynamic range at different values of Ω are carried out. Figure 7 shows the numerical calculation results for the nonlinear deviation ΔK in the ZLG with periodically reversed rectangular-shaped frequency bias with the amplitude 200 kHz and the capture range 1 kHz ($\Omega_0/\Omega_b \approx 5\times10^{-3}$). It is seen that $\Delta K = 5\times10^{-4}$, and for $\Omega = \Omega_b$ we have $\Delta K = 0$. In Fig. 7 the approximating analytical expressions are shown that correctly describe the behaviour of ΔK at angular velocities far from the singular point $\Omega = \Omega_b$.

The nonlinear character of the frequency characteristic is most pronounced at the angular velocities of the true rotation in the vicinity of Ω_b [29, 30]. In this zone the frequency depen-

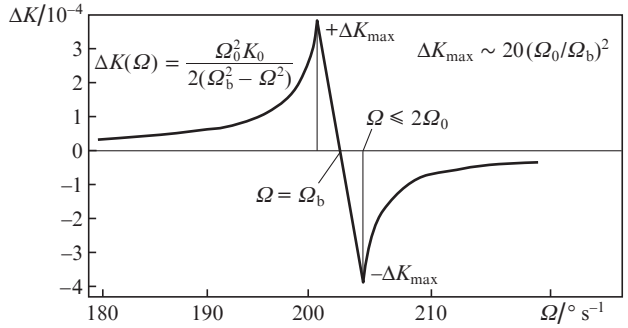

Figure 7. Theoretical dependence of scale factor nonlinearity on the angular velocity near the bias frequency Ω_b.

dence of the scale factor undergoes an anomalous dispersion-like oscillation near the absorption frequency, which is a consequence of strong coupling of counterpropagating waves (Fig. 7). The amplitude of this oscillation grows with the increase in Ω_0 and depends on the shape of the frequency bias. We recall that in contrast to the lasers with vibrating suspension (dithering), where the implemented bias is purely sinusoidal, in Zeeman lasers that allow electronic control of the oscillation parameters and non-mechanical biasing, the dependence of the bias on the time can possess any shape, e.g., sinusoidal, meander-shaped, triangle, etc. For the meander-shaped bias the relative amplitude ΔK of the scale factor oscillation can be described using the expression [29, 30].

$$\Delta K \approx 20(\Omega_0/\Omega_b)^2. \tag{19}$$

The width of the scale factor essential nonlinearity region is nearly equal to two widths of the static capture zone.

The typical experimental dependence of the ZLG scale factor nonlinearity on the angular velocity of rotation at large capture frequencies (about 500 Hz) is shown in Fig. 8. This dependence is rather symmetric and the sign is changed near $\Omega = \Omega_b = 70\ ^\circ\ s^{-1}$ which is important for the practical exploitation of the gyroscope. Indeed, in practice the bias frequency corresponds to large angular velocities that are acquired by real objects only during short time periods, quickly returning to the region of small angular velocities, so that the contribution of this nonlinearity becomes practically zero. Due to this fact in the experiment it is rather difficult to reveal and record the scale factor nonlinearity zone.

For gyroscopes with improved cavity mirrors (the capture threshold smaller than 100 Hz) the scale factor nonlinearity near the bias frequency does not exceed 5×10^{-5} (Fig. 9).

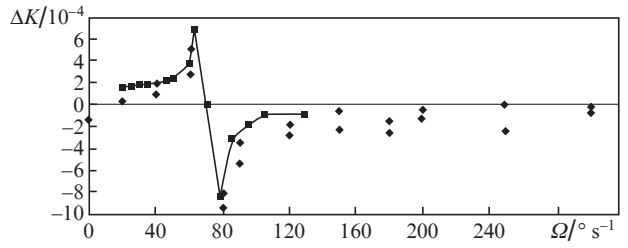

Figure 8. Typical dependence of the scale coefficient nonlinearity of the two-frequency ZLG (serial No. 0510328) on the frequency of its rotation at large (~500 Hz) capture frequencies [the points (◆) show the experimental results, the solid line plots the approximation] [29].

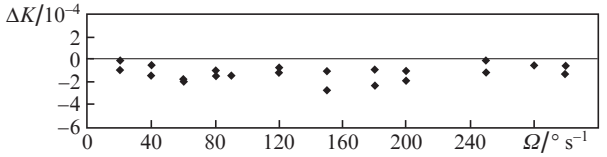

Figure 9. Experimental dependence of the relative scale factor of the ZLG (serial No. 0610350) on the angular velocity of rotation at small (~100 Hz) capture frequencies.

2.5. Specific features of the preliminary processing of ZLG information

By preliminary processing the information from a ZLG one can determine not only the angular velocity, but also other useful characteristics.

Calculating the difference and the sum of the number of interference fringes, recorded by the photodetector during the positive and negative half-periods of the frequency biasing, allows the determination of both the rotation angular velocity and the frequency bias amplitude. To count the interference fringes, the photodetector device generates an electric pulse each time an interference fringe passes the sensitive area. In addition to the above characteristics, in the four-frequency regime one can extract from the output signal the signal of cavity perimeter detuning and the signal, proportional to the residual magnetic field in the active medium.

In the two-frequency regime with a meander-shaped sign-changing frequency bias we obtain two sums of pulses during the period of the bias frequency variation, N^+ during the positive half-period and N^- during the negative half-period. They allow the calculation of the angular velocity Ω and the frequency bias Ω_b:

$$\Omega = (N^+ - N^-)/KT, \tag{20}$$

$$\Omega_b = (N^+ + N^-)/KT. \tag{21}$$

In the four-frequency regime during the period of the bias frequency variation T we obtain four sums of pulses, two for one mode, N^+ and N^-, and two for the other mode, $\tilde{N}^+$ and $\tilde{N}^-$. They allow the calculation of the angular velocity Ω, the mean frequency bias Ω_b, as well as the frequency signals of the perimeter detuning (f_y) and the residual magnetic field in the active medium (f_h):

$$\Omega = (N^+ - N^- - \tilde{N}^+ + \tilde{N}^-)/KT, \tag{22}$$

$$\Omega_b = (N^+ + N^- + \tilde{N}^+ + \tilde{N}^-)/KT, \tag{23}$$

$$f_y = (N^+ + N^- - \tilde{N}^+ - \tilde{N}^-)/T, \tag{24}$$

$$f_h = (N^+ - N^- + \tilde{N}^+ - \tilde{N}^-)/T. \tag{25}$$

Using the signal f_y one can stabilise the cavity perimeter to 10^{-3}–$10^{-4}\lambda$, and using the signal f_h it is possible to reduce the magnetic sensitivity to a few hundredths of a degree per hour. In the case of the two-frequency regime for stabilising the perimeter one has to use one more analogue signal, the modulation amplitude of the output signal of one of the counter-propagating waves A_y, proportional to the perimeter detuning.

The advantage of such perimeter tuning systems in the ZLG as compared to that in dithered gyroscopes is that they

do not require artificial modulation of the laser cavity perimeter that increases the random drift of the gyroscope zero.

3. Increasing the ZLG precision by the mode reverse method

The progress in electronics and algorithmic digital correction of the gyroscope output signals [30, 34, 35] made it possible to implement the so-called quasi-four-frequency (or mode reverse) regime of the gyroscope operation. In this regime the switching of orthogonally polarised modes is performed periodically with the interval of 1–5 min. Correspondingly, the information processing in the channels of angular velocity, frequency bias and residual magnetic field is performed like in the true four-frequency regime. The advantage of the regime with mode reverse over the true four-frequency regime is the significant simplification of laser construction, and the major drawback is the presence of short-time losses of information at the moments of mode switching. The present-day level of digital technique allows significant compensation of this drawback by restoration of the lost information basing on the output signal values before and after the mode switching.

Figure 10 presents the time dependence of the gyroscope zero displacement for each of the modes and the resulting output signal of the gyroscope in the mode reverse regime.

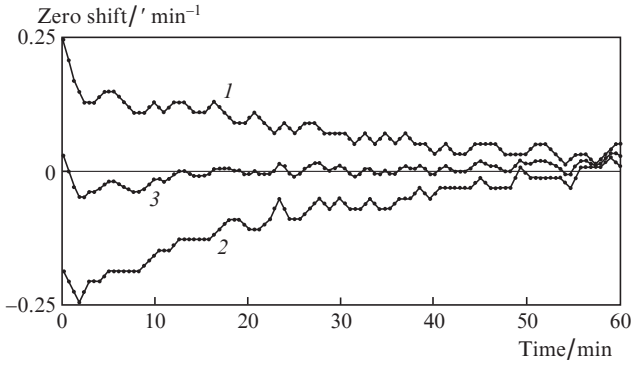

Figure 10. Temporal behaviour of the gyroscope zero shift for each of the two orthogonal modes (*1*, *2*) and the output signal of the gyroscope in the mode reverse regime (*3*).

The regime of mode reverse provides an additional valuable tool for a separate study of magnetic and nonmagnetic components of the gyroscope zero drift and for developing the measures aimed at their reduction. As an example, in Fig. 11 the time behaviour of nonmagnetic and magnetic components of the zero drift are presented separately. It is seen that the dominant contribution to the total drift of the gyroscope zero is due to the magnetic component, suppressed in the mode reverse regime.

In the process of gyroscope operation the main error is the error of the orientation angle, accumulated in the process of the object motion. The mode reverse regime allows essential reduction of this error, as demonstrated in Fig. 12. The accumulated errors of the angle measurement in the two-frequency regime are separately shown for each mode and in the mode reverse regime with calibration. During the first minutes, while the calibration has been performed, the signal in the mode reverse regime was assumed to be zero.

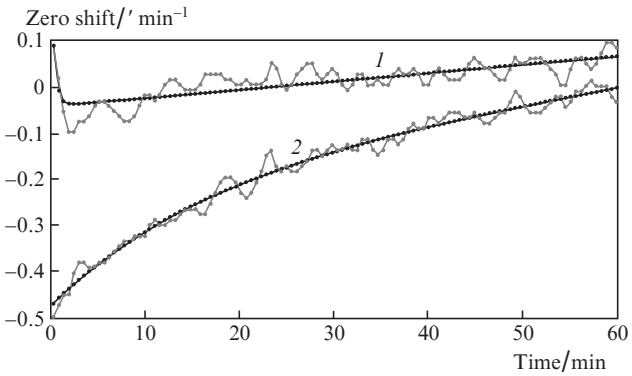

Figure 11. Temporal behaviour of nonmagnetic (*1*) and magnetic (*2*) component of zero shift.

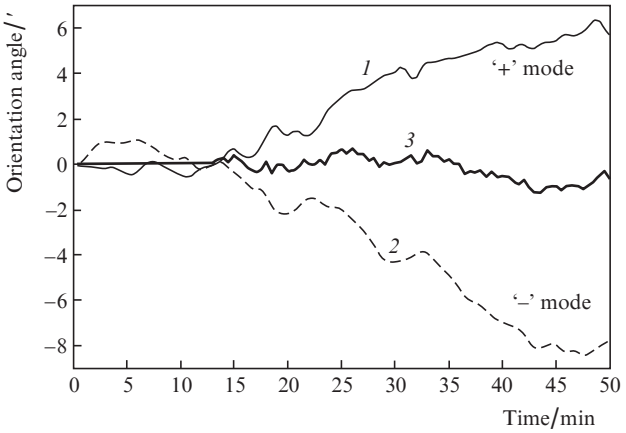

Figure 12. Temporal behaviour of the accumulated ZLG orientation angle measurement in the single-mode regime for each of the orthogonal modes (*1*, *2*) and in the mode reverse regime (*3*).

4. Practical implementation of ZLGs

To date a series of two-frequency and quasi-four-frequency laser gyroscope sensors with Zeeman-based magnetooptical control and three-axis laser gyroscopes on their basis are produced.

The exterior view of the ZLK series laser sensors is presented in Fig. 13. The ring cavity of the sensor is formed by four mirrors, three of which are planar and the fourth one is spherical (Fig. 14).

Two mirrors, located on one diagonal, are mounted on high-precision piezoengines for controlling and correcting the

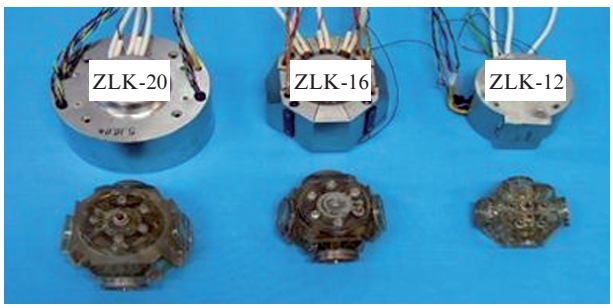

Figure 13. Produced Zeeman angular velocity sensors.

Table 1. Parameters of Zeeman laser gyroscopes.

Model	Scale factor/ ″ pulse^{-1}	Zero irreproducibility/deg h^{-1}		Zero shift starting instability/deg h^{-1}		Overall size/mm
		Two-frequency regime	Quasi-four-frequency regime	Two-frequency regime	Quasi-four-frequency regime	
MT-300	4.44	1.0–2.0	0.5–1.0	0.2–0.5	0.1–0.2	∅162×115
MT-401	3.33	0.5–1.0	0.2–0.3	0.1–0.2	0.03–0.05	∅180×140
MT-501	2.75	0.3–0.5	0.03–0.1	0.02–0.1	0.01–0.03	∅200×150

Figure 14. Cavity with mirrors.

cavity perimeter. The sensors of the ZLK series differ in the perimeter (from 120 to 200 mm), their monoblock cavities are made of glassceramic material with a super-low coefficient of thermal expansion. The cavity mirrors are mounted at the cavity body using the optical contact method, for which the base planes on the body and the surfaces of the mirror substrates are super-polished. The gas discharge is excited in all four arms of the cavity with pairwise opposite direction of current in them. The permalloy screen reduces the influence of external magnetic fields.

Three-axis ZLGs consist of three similar ZLK sensors, electronic units of sensor life sustenance and control and the unit of the output signal formation. The sensors and the electronic units are placed in a single hermetical construction with the external magnetic screen (Fig. 15).

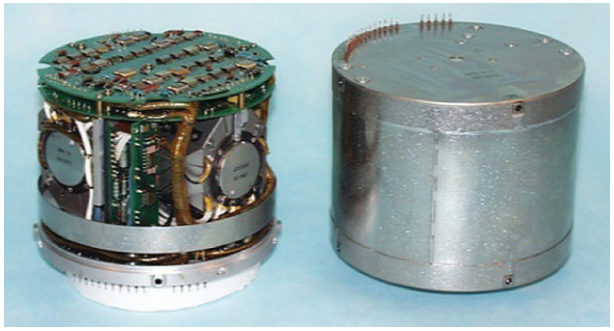

Figure 15. Unified construction of the three-axis ZLG MT-401 (right – assembled; left – with the case and screens removed).

The main ZLG parameters are summarised in Table 1, from which it follows that the zero shift instability in the mode reverse regime for the device MT-501 amounts to 0.01–0.03 deg h^{-1}, which is comparable with the precision parameters of a planar-contour LG with vibrating suspension.

To date the potentialities of small-dimension ZLGs are far from being exhausted. The reduction of intracavity losses and scattering by improving the quality of cavity mirrors (see, e.g., [36–45]), the reduction of the capture frequency, the improvement of fabrication and assembling accuracy, as well as the optimisation of laser parameters and operating regimes, including the algorithmic correction of the reproduced dependences of the zero drift on the temperature and other environmental conditions, allow the reduction of zero shift in the steady-state regime to 0.005–0.01 deg h^{-1}, the random deviation being as small as 0.003 deg h$^{-1/2}$, which will essentially extend the field of the considered ZLGs application.

Acknowledgements. The authors express their gratitude to Yu.Yu. Kolbas, Yu.A. Vinokurov, A.I. Yakushev, N.I. Khokhlov, A.Yu Golyaeva, M.I. Klimentova and other staff members of the gyroscope team at the Polyus Research Institute for their participation in preparing materials for this paper.

References

1. Mel'nikov A.V., Prosvetov V.K., Rybakov B.V., Skulachenko S.S., Khromykh A.M., Yudin I.N. USSR Patent No. 745242 with priority of 16.05.1967.
2. Rybakov B.V., Demidenkov Yu.V., Skrotskii S.G., Khromykh A.M. *Zh. Eksp. Teor. Fiz*., **57**, 1184 (1969).
3. Azarova V.V., Golyaev Yu.D., Dmitriev V.G., Mel'nikov A.V., Nazarenko M.M. in: *Nauchnye Trudy 2-i S.-Peterburgskoi mezhdunarodnoi konferentsii po giroskopicheskoy tekhnike* (Proc. Second Saint-Petersburg International Conference on Gyroscope Engineering (Saint-Petersburg: TsNII 'Elektropribor', 1995) p. 49.
4. Azarova V.V., Golyaev Yu.D., Dmitriev V.G., Melnikov A.V., in *Navigational Technology For The 3rd Millennium* (Cambridge, Massachusetts, 1996) p. 697.
5. Azarova V.V., Golyaev Yu.D., Dmitriev V.G., Mel'nikov A.V., Nazarenko M.M. *Giroskopiya i Navigatsiya*, No. 4 (19), 7 (1997).
6. Azarova V.V., Golyaev Yu.D., Dmitriev V.G., et al., in *Optical Gyros and Their Application* (France: RTO, 1999) p. 5-1.
7. Azarova V.V., Golyaev Yu.D., Dmitriev V.G., *Kvantovaya Elektron*., **30**, 96 (2000) [*Quantum Electron*., **30**, 96 (2000)].
8. Klimontovich Yu.L., Landa P.S., Lariontsev E.G. *Zh. Eksp. Teor. Fiz*., **52**, 1616 (1967).
9. Kuryatov V.N., Landa P.S., Lariontsev E.G. *Izv. Vyssh. Uchebn. Zaved., Ser. Radiofiz*., **11**, 1839 (1968).
10. Privalov V.E., Fridrikhov S.A. *Usp. Fiz. Nauk*, **97**, 377 (1969).
11. Pomerantsev N.M., Skrotskii G.V. *Usp. Fiz. Nauk*, **100**, 361 (1970).
12. Aronowitz F. In: *Laser Application* (New York: Academic Press, 1971) pp 133–200.
13. Bychkov S.I., Lukyanov D.P., Bakalyar A.I. *Lazernyi giroskop* (Laser Gyroscope) (Moscow: Sov. radio, 1975).
14. Chou W.W., Gea-Banacloche J., et al. *Rev. Modern Phys.*, **57**, 61 (1985).
15. Savelyev A.M., Solovyova T.I. *Zarub. Radioelektron*., (8), 77 (1981).
16. Wilkinson G.R. *Prog. Quantum Electron.*, **11**, 1 (1987).
17. Seregin V.V., Kukuliyev R.M. *Lasernye girometry i ikh primenenie* (Laser Gyrometers and Their Application) (Moscow: Mashinostroenie, 1990).
18. Khromykh A.M. *Elektron. Tekh., Ser. 11. Lasernaya Tekh. Optoelektron.*, No. 1 (53), 76 (1990).
19. Khromykh A.M. *Elektron. Tekh., Ser. 11. Lasernaya Tekh. Optoelektron*., No. 2 (54), 44 (1990).

20. Rybakov B.V., Skulachenko S.S., Khromykh A.M., Yudin I.I. *Zh. Eksp. Teor. Fiz*., **64**, 1146 (1973).
21. Khromykh A.M., Yakushev A.I. *Kvantovaya Elektron*., **4**, 27 (1977) [*Sov. J. Quantum Electron*., **7**, 13 (1977)].
22. Savelyev I.I., Khromykh A.M., Yakushev A.I. *Kvantovaya Elektron*., **6**, 1155 (1979) [*Sov. J. Quantum Electron*., **9**, 682 (1979)].
23. Savelyev I.I., Timonin P.V., Yakushev A.I. *Kvantovaya Elektron*., **6**, 1549 (1979) [*Sov. J. Quantum Electron*., **9**, 909 (1979)].
24. Savelyev I.I. *Kvantovaya Elektron*., **6**, 632 (1979) [*Sov. J. Quantum Electron*., **9**, 381 (1979)].
25. Mogil'naya T.Yu., Savelyev I.I., Timonin P.V., Yakushev A.I. *Kvantovaya Elektron*., **10**, 2032 (1983) [*Sov. J. Quantum Electron*., **13**, 1353 (1983)].
26. Nazarenko M.M., Savelyev I.I., Skulachenko S.S., Khromykh A.M., Yudin I.I. *Kvantovaya Elektron*., **4**, 1738 (1977) [*Sov. J. Quantum Electron*., **7**, 984 (1977)].
27. Savelyev I.I., Khromykh A.M. *Kvantovaya Elektron*., **3**, 1517 (1976) [*Sov. J. Quantum Electron*., **6**, 821 (1976)].
28. Bennett W.R., Jr. *The Physics of Gas Lasers* (New York: Gordon and Breach, 1977; Moscow: Mir, 1964).
29. Golyaev Yu.D., Golyaeva A.Yu., Nazarenko M.M., Tikhmenev N.V. *Kontsentrirovannye potoki energii* (Concentrated Energy Flows) (Moscow: MGU, 2006) p. 175.
30. Dmitriev V., Golyaev Yu., Kolbas Yu., Nazarenko M., Tikhmenev N., Vinokurov Yu. *Proc. 15th Intern. Conf. on Integrated Navigation Systems* (St. Petesburg, 2008) p. 127.
31. Klimontovich V.L. (Ed.) *Volnovye i fluktuatsionnye protsessy v lazerakh* (Wave and Fluctuation Processes in Lasers) (Moscow: Nauka, 1974).
32. Aronowitz F., in *Optical Gyros and Their Application* (France: RTO, 1999) p. 3-1.
33. Golyaev Yu.D., Kolbas Yu.Yu., Nayda O.N., Tolstenko K.A., Chubar' A.V. *Elektron. Tekh., Ser. 11. Lazernaya Tekh. Optoelektron*., No. 4 (52), 41 (1989).
34. Golyaev Yu.D., Dmitriev V.G., Kazakov A.A., Kolbas Yu.Yu., Nazarenko M.M., Tikhmenev N.V., Yakushev A.I. Russian Federation Patent No. 2408844 with priority of 07.10.2009.
35. Vinokurov Yu.A., Golyaev Yu.D., Dmitriev V.G., Kazalov A.A., Kolbas Yu.Yu., Tikhmenev N.V., Yakushev A.I. Russian Federation Patent No. 2418266 with priority of 11.01.2010.
36. Azarova V.V., Dmitriev V.G., Lokhov Yu.N., Malitskii K.N. *Kvantovaya Elektron*., **30**, 359 (2000) [*Quantum Electron*., **30**, 359 (2000)].
37. Kolodnyi G.V., Golyaev Yu.D., Azarova V.V., Rasyov M.M., Tikhmenev N.V. *Proc. SPIE Int. Soc. Opt. Eng.*, **4350**, 120 (2000).
38. Azarova V.V., Dmitriev V.G., Lokhov Yu.N., Malitskii K.N. *Kvantovaya Electron*., **31**, 740 (2001) [*Quantum Electron*., **31**, 740 (2001)].
39. Azarova V.V., Dmitriev V.G., Lokhov Yu.N., Malitskii K.N. *Opt. Zh*., **69**, 71 (2002).
40. Azarova V.V., Efremova N.A. *Kvantovaya Elektron*., **32**, 239 (2002) [*Quantum Electron*., **32**, 239 (2002)].
41. Azarova V.V., Asadchikov V.E., Zanaveskin M.L., Roshchin B.S., Grishchenko Yu.V., Tolstikhina A.L. *Kristallografiya*, **4**, 730 (2008).
42. Azarova V.V. In: *Tekhnologii obrabotki optocheskikh elementov i naneseniya vakuumnykh pokrytii* (Technologies of Optical Element Processing and Vacuum Coating Deposition) (Minsk: Kontenant, 2013) p. 8.
43. Azarova V.V. *Opt. Spektrosk*., **107**, 201 (2009).
44. Sidoryuk O.E., Azarova V.V., Golyaeva A.Yu., Lobanov P.Yu., Manuilovich I.S., Rasev M.M. In: *Lazery, izmereniya, informatsiya* (Lasers, Measurements, Information) (St-Petersburg: St-Petersburg State Polytechnic University, 2012) Vol. 2, p. 303.
45. Gorshkov V.N., Azarova V.V., Petrukhin E.A. In: *Lazery, izmereniya, informatsiya* (Lasers, Measurements, Information) (St-Petersburg: St-Petersburg State Polytechnic University, 2012) Vol. 2, p. 81.